Front-End Parameter Identification for Performance Optimization and Load Voltage Regulation of Detuned Wireless Power Transfer Systems

Ali Zakerian, Sohrab Abbasian, *Graduate Student Member, IEEE*, Prasad Jayathurathnage, *Senior Member, IEEE*, Tomi Roinila, *Member, IEEE*, Marcelo Godoy Simões, *Fellow, IEEE*, and Paavo Rasilo, *Member, IEEE*

***Abstract*—The technology of wireless power transfer (WPT) has been in accelerated adoption for charging battery-powered devices, particularly in electric vehicles. The variable coupling coefficient between the transmitter and receiver coils and variable equivalent load resistance are the factors affecting the system's operation. In addition, it is not feasible in practice to perfectly match the resonance frequencies of transmitter and receiver circuits due to parameter variation, rated component tolerances, and manufacturing mismatches. The authors investigated a new system identification method based on nonlinear fitting in order to improve the issues related to parameter uncertainty. The operation is enhanced by employing a frequency control methodology to regulate the load voltage. The system is optimized for zero voltage switching (ZVS) and low conduction loss by the frequency control algorithm to keep the operation efficient. This article shows a very cost-effective and simple measurement of the transmitter's current magnitude and detection of parameter changes to achieve the new optimum operating point under the dynamic operating conditions. The effectiveness of the proposed method has been validated in the laboratory with experimental results from a prototype, confirming the theoretical analysis and design.**

***Index Terms*—Mutual coupling, system identification techniques, voltage control, wireless power transfer (WPT), zero voltage switching (ZVS).**

I. Introduction

WIRELESS power transfer (WPT) technology has been widely studied during the past decade. WPT contributes to the safe, reliable, and easy charging of battery-powered devices. Electric vehicles can be charged while they are moving by employing dynamic WPT [1].

There are practical issues to be addressed to make WPT systems a justifiable substitution for cable-based chargers. It is desired to keep the system efficiency and output power high enough, while there is a large air gap between the transmitter and receiver coils. The goal can be achieved by optimal coil design [2], compensation circuit design [3], or control methods [1], [4]. Within the last option, the proposed methods can be categorized into optimal point tracking-based and parameter estimation-based schemes. In [5], [6], [7], and [1], high efficiency or high input power factor has been tracked by variable frequency control. On the other hand, the parameter estimation methods have been proposed in [8] and [9].

In a recent study, a double-layer pulsewidth pulse frequency-based optimal control was proposed to track the maximum energy efficiency and provide constant voltage and current to the load [7]. Measurements of load voltage, rectifier voltage, and load current are needed to deliver to the transmitter-side controller. The method needs a data communication link between the transmitter and receiver sides that diminishes system reliability and increases system cost and complexity. This issue is addressed in the method proposed in [8]. As the input impedance of the WPT system is analyzed for the estimation of the mutual inductance, the data communication link is eliminated. The operation starts with an initial frequency that does not turn the rectifier diode on to estimate the mutual inductance regardless of the load impedance. However, the defined initial frequency directly depends on the battery's nominal voltage. The rectifier may turn on if another device with a different nominal battery voltage is connected to the charger and the predefined initial frequency is applied. On the other hand, the method is not effective if the mutual inductance changes during operation. Both problems of data communication link and phase measurement are addressed in a recent study proposing a new mutual inductance estimation method for multiple transmitters and series compensated systems [9]. The method does not need the data communication link. Only fundamental of transmitter-side voltages and currents is needed for the estimation. First,

Received 24 October 2024; revised 15 January 2025, 17 April 2025, and 18 June 2025; accepted 9 July 2025. Date of publication 16 July 2025; date of current version 3 October 2025. This project has received funding from the European Research Council (ERC) under the European Union's Horizon 2020 research and innovation programme (Grant agreement No 848590). Recommended for publication by Associate Editor Huang-Jen Chiu. *(Corresponding author: Ali Zakerian.)*

Ali Zakerian, Sohrab Abbasian, Tomi Roinila, and Paavo Rasilo are with the Electrical Engineering Unit, Tampere University, 33014 Tampere, Finland (e-mail: ali.zakerian@tuni.fi; sohrab.abbasiankasehgari@tuni.fi; tomi.roinila@tuni.fi; paavo.rasilo@tuni.fi).

Prasad Jayathurathnage is with the Danfoss Drives and the Department of Electrical Engineering and Automation, School of Electrical Engineering, Aalto University, 02150 Espoo, Finland (e-mail: prasad.k.sampath@ieee.org).

Marcelo Godoy Simões is with the School of Technology and Innovations, Electrical Engineering, University of Vaasa, 65200 Vaasa, Finland (e-mail: marcelo.godoy.simoes@uwasa.fi).

Color versions of one or more figures in this article are available at https://doi.org/10.1109/JESTPE.2025.3589548.

Digital Object Identifier 10.1109/JESTPE.2025.3589548

the ratios of mutual inductances are calculated. Then, they are used for the calculation of the exact values of mutual inductances. Therefore, it cannot be used for single transmitter systems. Moreover, it is assumed that the load resistance value is known for the controller. Yet, it is a time variable parameter and unknown to the transmitter-side controller.

Keeping the load voltage constant at a given reference value is a requirement for WPT systems. For example, in battery charging applications, the equivalent load resistance changes with the battery state of charge. Employing a transmitter-side dc–dc converter has been proposed in [10]. In [11], the necessity of the additional dc–dc converter is eliminated by tuning the duty ratio of the transmitter-side inverter. However, a data communication link between the transmitter side and receiver side is needed for using the load voltage feedback in the transmitter-side controller. The same problem exists in a recent study, wherein constant load voltage and current are realized by tuning the reference duty ratio using a self-oscillating algorithm [7]. Controlling the duty ratio of the receiver-side dc–dc converter's switches is proposed in [6]. A frequency tracking approach is used to maximize the system efficiency by finding the operating point at which the phase difference between inverter voltage and current is zero. However, every operating point corresponding to zero phase angle does not necessarily result in maximum efficiency. Depending on circuit parameters, the frequency response input phase angle may cross 0° three times. Among those operating points, only the middle one corresponds to the maximum efficiency. The article [6] studied multiple transmitter WPT systems, and phase measurement of the transmitter current is necessary for optimization, which may become complicated and expensive for high-frequency waveforms. In [12], the load voltage regulation is realized by controlling a transmitter-side dc–dc converter. On the other hand, a receiver-side semi-bridgeless active rectifier provides optimal load impedance. For this purpose, a dual-side control strategy is proposed in [12] for a WPT system, including LCC compensation configuration at the both sides. However, it requires a data communication link between the transmitter and receiver sides. Moreover, the variation of the coils' coupling coefficient during operation is not considered in the control method.

The operating frequency is a decisive factor in WPT systems as the operation is based on resonant effect created by the coil's inductance and the compensation capacitance. It is known that operation at the resonant frequency of the receiver side ($f_{R,r}$) results in the highest efficiency in series–series-compensated WPT systems [1]. If the resonant frequency of the transmitter side ($f_{T,r}$) is equal to $f_{R,r}$, which is called the tuned case, the operation at the common resonant frequency results in the unity power factor as well. Yet, soft switching of the high-frequency inverter is not realized by the mentioned frequency.

The criteria adopted for the past few years is tuning both sides' resonant frequencies by designing $f_{T,r} = f_{R,r}$. However, detuned WPT systems with $f_{T,r} \neq f_{R,r}$ have been investigated in many recent studies [1], [3], [4], [13], [14], [15], [16], [17], [18]. Detuning caused by the aging effect and circuit parameter tolerance affects system operation significantly.

In order to avoid high inverter current when the coupling coefficient k decreases or load resistance increases, a detuned CLL-series compensation has been proposed in [13]. It is shown that the detuning rate of the transmitter circuit can be set adequately to avoid overcurrent issue. Dealing with the same issue, a comprehensive analysis of detuning has been given in [14]. As a result, a design approach has been proposed for detuned series–series-compensated WPT systems. The goal of stable output current with variable k and load resistance has been sought for LCC-series-compensated WPT systems by detuning the transmitter circuit in [3]. Although the methods given in [3] and [14] contribute to constant power transfer against a wide range of k variation, the power transfer level and efficiency achievable in tuned systems are sacrificed. In another study, the detuned LCC and series compensation are combined together [15] to widen the range of optimum k. Therein, the compensation of the transmitter circuit is shifted between LCC and series by using a switch at the transmitter side, which is determined by a predefined k threshold. The mode selection of the switch is carried out by observing the load current in practice.

Switch-controlled capacitors (SCCs) have been employed in several studies to deal with detuning [4], [16], [17]. The constant optimum load corresponding to the system's maximum efficiency has been sought in [17] by changing the resonant frequency of both sides. The goal is realized by switching series capacitors using power electronic MOSFETs. Among the two proposed implementations, it is shown that the half-wave modulation results in higher efficiency than the full-wave one. The variable capacitors are used in series with conventional capacitors in [16]. The transmitter side is controlled to realize zero input phase angle, while the receiver one is adjusted to track the minimum power. The idea has been employed in LCC–LCC-compensated systems in [4]. SCC is implemented in series to the filter inductor on both the transmitter and receiver sides in order to increase the input power factor and regulate the load voltage. Although all of the mentioned methods would improve the system performance, adding extra switching components is not desirable regarding system cost and control complexity. Without adding any extra components, an optimum frequency tracking method has been applied to deal with the detuning issue in [1]. It has been observed that the power factor drops significantly if the detuned system is operated at the conventional operating frequency. Thus, a novel figure of merit considering both system efficiency and power factor has been proposed in [1]. The issue of low power factor in detuned systems is also elaborated in [18]. However, the provision of soft switching conditions is not ensured for all of the possible cases in both of those. A model predictive control scheme has been proposed to adjust the operating frequency, so that the power factor becomes one. Yet, the method needs phase measurement and does not consider soft switching operation.

In [19], the constant load voltage is provided by controlling a switched-capacitor active half-wave rectifier. It is shown that the output voltage is regulated even with the changes of load resistance and coupling coefficient during operation. The system does not need a data communication link between

TABLE I
COMPARISON OF THE PROPOSED METHOD WITH RELEVANT LITERATURE

criteria	**[1]**	**[6]**	**[12]**	**[15]**	**[16]**	**[17]**	**[19]**	**[20]**	**Proposed method**
Not requiring high sampling rate measurement	✓	×	×	✓	×	✓	×	✓	✓
No additional power switches needed	✓	×	×	×	×	×	×	×	✓
Detuning of resonance frequency considered	×	×	×	×	✓	✓	×	✓	✓
No need for data communication between Tx- and Rx-sides	×	✓	×	×	✓	×	✓	×	✓
No tracking of the operating point directly from the measurements	×	×	✓	✓	✓	×	✓	✓	✓
Possibility to control load voltage or power	×	✓	✓	✓	✓	✓	✓	✓	✓
ZVS of all switches are guaranteed	×	✓	✓	✓	×	✓	×	✓	✓
Able to deal with dynamic change of k	×	×	×	✓	✓	×	✓	✓	✓
Compensation type	S-S	S-S	LCC-LCC	S/LCC-S	SCC	SCC	S-S+SCC	LCC-LCC+SCC	S-S
Stabilization time	2 s	20 ms	0.5 s	N/A	N/A	150 ms	2 s	28 ms	2 s

the transmitter and receiver. However, adding the required MOSFET and other circuit components in the transmitter side rectifier results in a higher cost of the system. On the other hand, the zero-voltage switching (ZVS) operation is provided only for the receiver-side MOSFET, while the soft switching consideration is not taken into account for the transmitter-side inverter switches. It is assumed that both the transmitter- and receiver-side circuits operate at the resonant frequency. However, the assumption is not valid while there is detuning in the system. Using SCC in an LCC–LCC-compensated WPT system is proposed in [20]. A dual-phase shift method has been proposed to realize ZVS for all switches as well as regulate the load voltage. However, a data communication link is needed between the transmitter and receiver. Moreover, employing the SCC and semi-active rectifier at the receiver side increases the capital cost of the system. A concise comparison of the most relevant methods based on the specified criteria is presented in Table I. The review of the literature reveals that no control method has yet satisfied all of these criteria. Consequently, this article proposes a novel performance optimization and voltage regulation method to address these requirements. It is seen that the proposed method is slower than some of the available ones in the literature. In fact, those do not include estimation methods. The other listed advantages of the proposed method are thus achieved at the expense of a slower control.

The effects of the detuned transmitter and receiver resonant frequencies and variable coupling coefficient on the WPT system load voltage are analyzed in this article. An estimation method based on nonlinear fitting is proposed to determine the system parameters, including the coupling coefficient, the equivalent load resistance, and the receiver-side compensation capacitance. Then, a variable frequency control method is proposed to achieve three goals, including regulation of the load voltage, realizing the soft-switching of the inverter switches, and lowering the condition power loss in the system. The fact that no extra converters are employed in the system makes the idea cost-effective. As the method needs only the magnitude of the transmitter current, the issues of employing additional sensors, phase measurements, and a data communication link between the two sides are avoided. Furthermore, the system is able to deal with the variations of parameters during the operation and update the optimum applied frequency based on the new estimation. On the other hand, the proposed method can detect detuned cases and deal with them as well as the tuned case. This makes the system operation reliable and efficient in practice. The effectiveness of the proposed method is validated using the experimental results obtained from a laboratory WPT setup. Moreover, the experimental results from the control system operation under sudden variations of coupling coefficient and load resistance are presented.

The rest of this article is structured as follows. The circuit model of WPT system and the analytical modeling based on equations and mathematical analysis are presented in Section II. In Section III, the load voltage and efficiency of tuned and detuned WPT systems are elaborated. A novel control method composed of parameter estimation, load voltage regulation, and performance optimization is presented in Section V. The effectiveness of the proposed method is assessed in Section VI using the experimental results. This article is concluded in Section VII.

II. SYSTEM MODEL

A schematic model of the studied WPT system with series compensation at the transmitter and receiver sides is shown in Fig. 1.

The circuit equations of the transmitter and receiver sides are

$$U = Z_{\mathrm{T}} i_{\mathrm{T}} - j\omega M i_{\mathrm{R}} \tag{1}$$

$$j\omega M i_{\mathrm{T}} = (R + Z_{\mathrm{R}})\, i_{\mathrm{R}} \tag{2}$$

where i_{T} and i_{R} denote the rms phasor of the transmitter- and receiver-sides' fundamental currents, respectively. U is the root mean square-valued phasor of the inverter fundamental voltage with 180° duty ratio. Its magnitude $|U|$ is defined based on the dc link voltage V_{dc} as

$$|U| = \frac{2\sqrt{2}}{\pi} V_{\mathrm{dc}}. \tag{3}$$

The impedances of the transmitter and receiver circuits, Z_{T} and Z_{R}, are defined as

$$Z_{\mathrm{T}}(f) = r_{\mathrm{T}} + j\left(2\pi f L_{\mathrm{T}} - \frac{1}{2\pi f C_{\mathrm{T}}}\right) \tag{4}$$

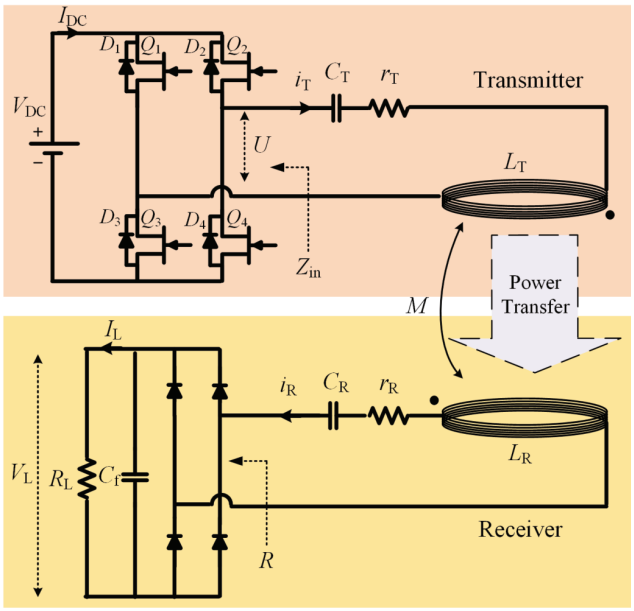

Fig. 1. Schematic view of a WPT system with series compensation capacitors at transmitter and receiver sides.

$$Z_R(f) = r_R + j\left(2\pi f L_R - \frac{1}{2\pi f C_R}\right) \tag{5}$$

respectively, where f, L_T, L_R, r_T, r_R, C_T, and C_R denote the operating frequency, transmitter coil inductance, receiver coil inductance, transmitter coil series resistance, receiver coil series resistance, the capacitance of transmitter series compensation, and capacitance of receiver series compensation, respectively. R is the equivalent load resistance seen from the rectifier. In [1], it is given as a function of the load resistance R_L by

$$R = \frac{8}{\pi^2} R_L. \tag{6}$$

The mutual inductance M is defined as a function of the coupling coefficient, L_T and L_R as

$$M = k\sqrt{L_T L_R}. \tag{7}$$

In this article, the magnitude of input impedance seen from the front end of the resonant circuit $|Z_{in}|$ is measured and analyzed for the sake of system identification. Using (1)–(5), (6), and (7), the input impedance of the system is given as

$$|Z_{in}(f,k,R)| = \left|\frac{U}{i_T}\right| = \left|Z_T(f) + \frac{(2\pi f k\sqrt{L_T L_R})^2}{R + Z_R(f)}\right|. \tag{8}$$

System efficiency is an indispensable performance criterion of WPT systems. The overall efficiency η_t is given as

$$\eta_t = \eta_{inv}\,\eta_{ac}\,\eta_{rec} \tag{9}$$

where η_{ac} denotes the efficiency of the ac resonant circuit and given as

$$\eta_{ac} = \frac{4\pi^2 f^2 M^2 R}{4\pi^2 f^2 M^2 (R + r_R) + r_T |R + Z_R(f)|^2} \tag{10}$$

where η_{inv} and η_{rec} represent the efficiency of the inverter at the transmitter side and the efficiency of the rectifier at the receiver side. In both converters, power loss can be categorized into conduction loss and switching loss.

III. Analysis of System Load Voltage and Efficiency

A WPT system should provide the required load voltage at its output to supply a battery or some other loads. Therefore, it is required to regulate the load voltage at its reference. In this section, the load voltage profile and its dependency on system parameters are analyzed. The load voltage is provided by the receiver-side rectifier. Assuming that the rectifier capacitance is large enough to filter the ripples, the load voltage can be written as a function of V_o, the voltage across the back end of the resonant circuit

$$|V_o| = R|i_R| = \frac{2\sqrt{2}}{\pi} V_L. \tag{11}$$

On the other hand, the receiver-side current can be written as

$$|i_R| = \frac{2\pi f M}{|Z_R(f) + R|} \frac{|U|}{Z_{in}(f,k,R)}. \tag{12}$$

Using (11) and (12), the load voltage is obtained as

$$V_L = \frac{2\pi f R M}{\left|Z_T(f)[Z_R(f) + R] + 4\pi^2 f^2 M^2\right|} V_{dc}. \tag{13}$$

As expected, it is seen that the load voltage is proportional to the input dc link voltage. The effect of the resonant circuit operation on the load voltage can be identified by the voltage gain of the system given by

$$G = \frac{V_L}{V_{dc}} = \frac{\frac{2\pi f R M}{\left|\left(r_T + j\left(2\pi f L_T - \frac{1}{2\pi f C_T}\right)\right)\right|}}{\left|\left(r_R + R + j\left(2\pi f L_R - \frac{1}{2\pi f C_R}\right)\right) + 4\pi^2 f^2 M^2\right|}. \tag{14}$$

It is seen that several system parameters, including operating frequency, mutual inductance, and equivalent load resistance, affect G. The effect will be analyzed in Section III-B. Using the series–series compensation, the resonant frequency of the transmitter and receiver sides is defined as

$$f_{T,r} = \frac{1}{2\pi\sqrt{C_T L_T}} \tag{15}$$

$$f_{R,r} = \frac{1}{2\pi\sqrt{C_R L_R}} \tag{16}$$

respectively. A tuned system is defined as a system, in which $f_{T,r} = f_{R,r}$. Usually, WPT systems are designed, so that the resonant frequency of the transmitter and receiver sides is identical. However, the equality may not be always valid in practice due to the following reasons.

1) It is obvious that $f_{T,r}$ and $f_{R,r}$ are the functions of circuit parameters that always have a tolerance. Therefore, it is possible that the desired value and the actual value of a circuit parameter are different.
2) The circuit parameters may change due to aging effect. Even if the resonant values are identical at the beginning of system operation, they may not be equal after years, necessarily.
3) For many applications of WPT systems, it is desired that one transmitter system charges several receivers one at a time. In this case, a reference resonant frequency is defined to make all potential receivers compatible.

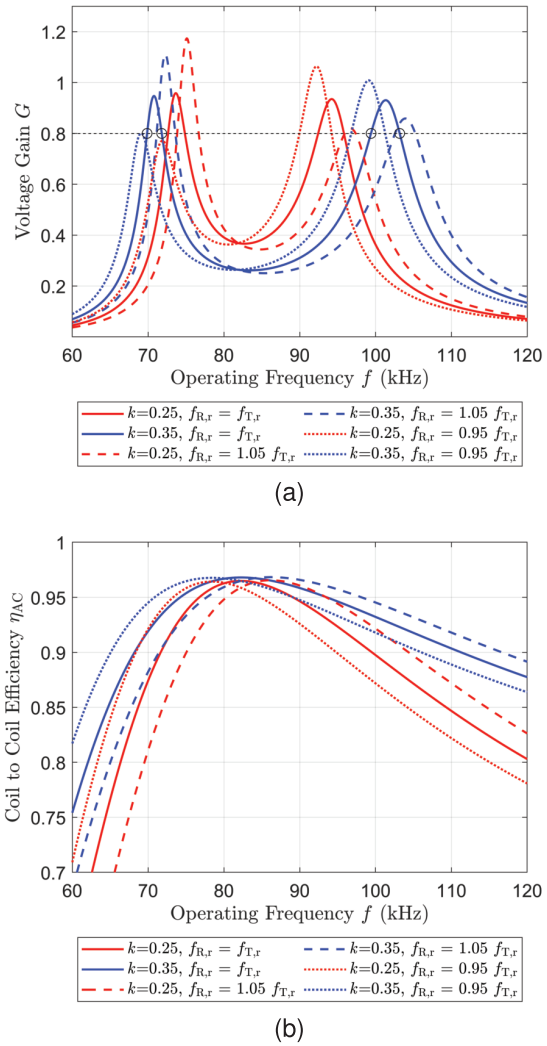

Fig. 2. Operation comparison of tuned and detuned systems versus operating frequency for different coupling coefficients. (a) Voltage gain. (b) Efficiency of the resonant circuit.

Yet, it is too ideal to assume that all of the potential receivers have exactly the same resonance frequency. For example, SAEJ2954 has defined a range of 81–90-kHz resonant frequency for WPT systems [1]. Hence, it can be understood that under a specific standard, there would be receivers with different resonant frequencies.

A detuned system is defined as a system in which $f_{T,r} \neq f_{R,r}$. In order to address the practical issues raised by detuning effect, the case is analyzed in this article as well as tuned systems.

A. Tuned System

The profiles of voltage gain and η_{ac} are shown in Fig. 2(a) and (b) with solid line, respectively. The figures are obtained using the parameters given in Table II. It is noteworthy that the parameters are selected based on the method given in [21] to provide a resonant frequency in the range of 80–85 kHz and a load voltage of 40 V. As expected, G depends on the coupling coefficient. The effect is significant in the vicinity of the resonant frequency, especially within $\pm$20 kHz. The effect is less significant outside of the range. The efficiency profile gets maximum at the common resonant frequency. It is noteworthy that the change of η_{ac} versus operating frequency is not as significant as that of G.

TABLE II
SYSTEM PARAMETERS

Parameter	Description	Value
L_T	Inductance of the transmitter coil	170 μH
L_R	Inductance of the receiver coil	170 μH
C_T	Capacitance of the transmitter circuit	22.2 nF
C_R	Capacitance of the receiver circuit	22.1 nF
f_T	Resonant frequency of the transmitter circuit	81.8 kHz
f_R	Resonant frequency of the receiver circuit	82.0 kHz
r_T	Resistance of transmitter coil	0.38 Ω
r_R	Resistance of receiver coil	0.24 Ω
R_L	Load resistance	11 Ω

B. Detuned System

In order to compare tuned versus detuned cases, the profiles of voltage gain and η are demonstrated in Fig. 2, where the dashed and dotted lines present cases in which $f_{R,r}$ is 5% higher and lower than $f_{T,r}$, respectively. It is seen that even a small detuning leads to considerable change in the G profile. As expected, the frequency corresponding to maximum η_{ac} changes when $f_{r,R}$ changes with detuning in Fig. 2(b). The optimum frequency shift is reflected in the change of η_{ac} in other operating frequencies at a constant rate.

C. Load Voltage Regulation by Frequency Control

The necessity of providing a constant load voltage is discussed in Section I. It is observed in Fig. 2(a) that the voltage gain is affected by detuning and variable coupling coefficient. Applying a voltage regulation control can keep the load voltage at its reference in spite of the change in system parameters like k. In this article, the operating frequency of the system is proposed to be controlled in a way that the load voltage is regulated. The frequencies realizing a reference voltage gain are determined by the interceptions of the load voltage profile in Fig. 2(a) and a horizontal line with a y-intercept of the desired G. For example, a horizontal line at $G = 0.8$ is drawn in Fig. 2(a) and the corresponding interceptions are shown. It is seen that four operating frequencies exist that realize $G = 0.8$.

Choosing the operating frequency in order to provide a specific load voltage will result in efficiency values less than maximum efficiency, as shown in Fig. 2(b). However, it is observed that the drop in η is not as significant as the change of G, while failure to provide the required load voltage results in aborting the charging process. On the other hand, it is seen that the η value is high enough for the most frequencies in the range shown in Fig. 2. Therefore, providing the required voltage is set as a higher priority than the maximum η in this article. It is needed to determine what the optimum frequency is among the four intercepted frequencies. In this article, the optimum frequency is selected based on the possibility of realizing soft switching and low phase displacement between inverter current and voltage ϕ. It is defined as

$$\phi = \arctan\left(\frac{\mathrm{Im}\{Z_{in}\}}{\mathrm{Re}\{Z_{in}\}}\right). \tag{17}$$

In this way, high η is achieved as well as load voltage regulation. These criteria are elaborated in Sections IV and V.

IV. Soft Switching Considerations

The power loss in the WPT system is caused by the inverter switches and conduction loss in the windings. The power loss inside the inverter is constituted by the conduction power loss and switching power loss of its MOSFETs. It is known that a lower amount of current results in lower conduction power loss not only inside each MOSFETs but also inside transmitter and receiver windings. Therefore, operating at a low ϕ contributes to increasing the overall η. The operating frequency of resonant converters can be set in a way that ZVS or zero current switching is realized. In this study, as the duty ratio of the inverter is always 180°, the lagging output current of the inverter $\phi > 0°$ ensures ZVS operation [15]. A contour of the phase angle of the input impedance ϕ is shown in Fig. 3(a). The plot is obtained using (17) and parameters given in Table II. Although the contours are plotted for the tuned case, the discussion is valid for the detuned cases, too.

As it is seen in Fig. 3(a), the phase angle gets negative and positive values in the operating frequency range for each k. There are two positive phase angle and negative phase angle regions for each k. Therefore, the whole area is broken down into the four regions shown in Fig. 3(a) specified by A, B, C, and D. The boundaries of the regions are the solid lines corresponding to zero phase angle. In Section V of this article, the lower and upper limits of the optimum frequency are defined as 0° and 30°, respectively. Therefore, a dashed curve corresponding to 30° is added to Fig. 3(a), too. It is seen that positive phase angles are realized in Regions B and D, while A and C are composed of operating points with negative phase angles.

The positive phase angle in series–series-compensated systems results in ZVS of the MOSFETs. On the other hand, zero current switching is realized by the negative input phase angle. Referring to Fig. 3(a), it is seen that operation at Regions A and C results in zero current switching, while ZVS is desirable in WPT systems. Therefore, Regions B and D include the desired operating points considering soft switching. For a given amount of active power, a smaller phase angle contributes to lower conduction power loss in the switches and lower power loss in the windings. Hence, the parts of Regions B and D, which are shown with light red, can be the desired choice regarding η. In practice, a threshold for ϕ should be defined that ensures low conduction loss as well as ZVS realization. In this article, the upper threshold is set at 30°, while it can be chosen based on each system's requirements. The lower limit should be set at 0° for ZVS realization. It is also desired to study the mentioned operating points in relation of their corresponding G. A contour of voltage gain is presented for the same operating frequency and k range in Fig. 3(b). The obtained regions in Fig. 3(a) are projected on Fig. 3(b), too. It is noteworthy that the points with higher G shown by dark red in Fig. 3(b) correspond to the boundaries between Regions A and B and between Regions C and D in Fig. 3(a). On the other hand, the lowest G values shown by light red in Fig. 3(b) correspond to the boundary between Regions B and C. It was previously mentioned that the desired operating points regarding the low system power loss were located around the boundary of the regions, too. Therefore, they correspond to the extremum points of G, as shown in Fig. 3(b).

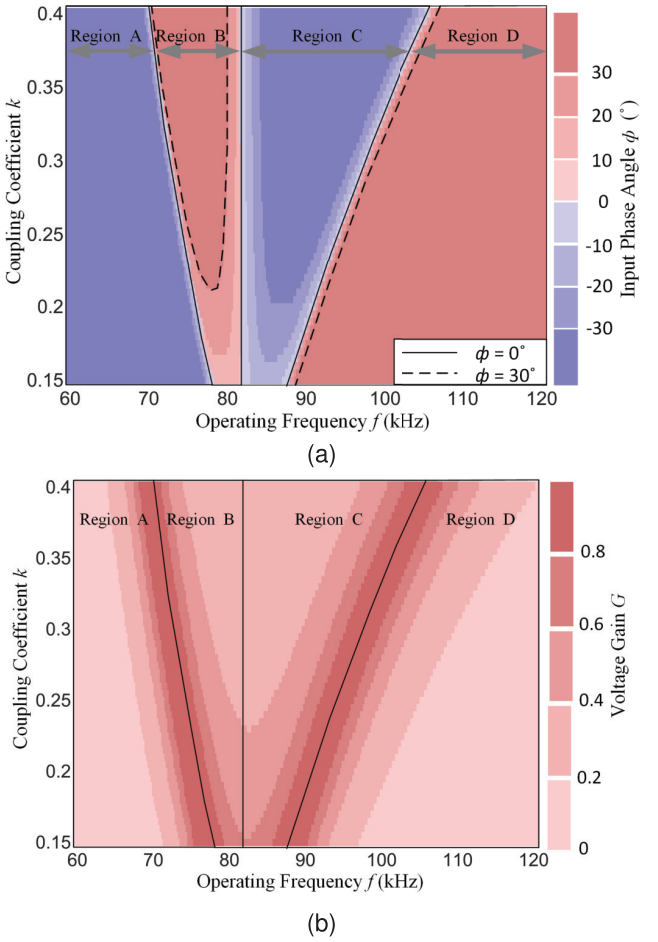

Fig. 3. Contours of system operation broken down to four possible operating regions based on the input impedance phase angle for a tuned WPT system in different operating frequencies and coupling coefficients. The boundaries between the regions are the curves corresponding to zero phase angle. (a) Input impedance phase angle. (b) Voltage gain.

The mentioned coincidence shows that both the maximum and minimum points shown in Fig. 2(a) can be considered as optimum operating points. Among them, it is better to set the desired G around the maximum possible G to use the full capacity of the power transfer.

V. Parameter Estimation and Frequency Control

As seen in Section III, system parameters change η and voltage gain, significantly. In the meantime, it is desired to have a constant V_L and high η even with unknown and variable parameters. In this article, it is assumed that V_{dc} is constant. Therefore, adjusting G is equivalent to adjust V_L. It is also assumed that k and R_L are unknown parameters that can change in time. As a realistic assumption, the changing rate of the parameters is considered to be slower than the switching period. The effect of detuning is also reflected by assuming that C_R at (16) is unknown. The rest of the parameters are

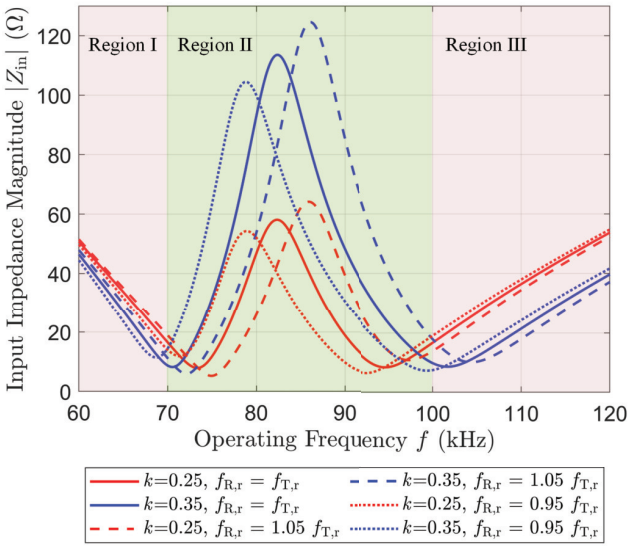

Fig. 4. Input impedance of the system versus operating frequency for different values of k, tuned and detuned cases. The whole bandwidth is divided into three regions to ease the proper selection of the test frequencies.

assumed to be known. Thus, the values of k, R_L, and C_R are required to be estimated. It is noteworthy that the transmitter-side parameters can be measured during regular maintenance to maintain the charging infrastructure reliability for the usage of different vehicles. The old components can be replaced if they are out of order. Using the data measured during maintenance, the receiver-side parameters can be updated in the control system if a change is observed in them. Therefore, the proposed estimation method will be able to perform well in this case, too.

An identification method is proposed in this section to estimate system parameters. Then, a frequency control method is proposed in this article to achieve the load voltage regulated at its reference value V_L^* as the first priority. In addition, the power loss of the inverter and the windings should be minimized.

A. System Identification and Parameter Estimation Method

In Fig. 4, $|Z_{in}|$ is plotted versus operating frequency using (8). The effects of different values of k and detuning are depicted in Fig. 4. For a better analysis, the horizontal axis is divided into three frequency ranges: Regions I–III. In Region I, almost all of the curves are close together, which means that the effect of k and detuning is not reflected in $|Z_{in}|$. In Region III, the curves corresponding to the same k are close together. Thus, it can be concluded that the effect of detuning is not visible by observing $|Z_{in}|$. Meanwhile, only k affects $|Z_{in}|$ values in this region. In Region II, it is seen that the curves are not close to each other.

It is observed that for this range of operating frequencies, which is around $f_{T,r}$ and $f_{R,r}$, k has a significant effect on the input impedance. For a given k, the profiles of the input impedance for detuned cases are different. For the higher k value, the peak point is higher. On the other hand, the effect of detuning caused the curves' maximum point to be shifted to a higher frequency for higher $f_{R,r}/f_{T,r}$ ratios. Therefore, the effects of both detuning and variable k are reflected well in $|Z_{in}|$ in Region II.

Overall, it is seen that the input impedance changes with different parameters in Region II. In this article, this effect is used to identify system parameters k, R_L, and C_R. Test frequencies are applied to the system, and the corresponding $|Z_{in}|$ values are recorded. Then, (8) is fitted to the measured points, considering k, R_L, and C_R as unknown parameters. Through this fitting, these unknown values are estimated.

As there are three unknown parameters in this problem, applying (8) at three different test frequencies can lead to an estimation of the unknown parameters. Yet, validation with more test frequencies will result in better accuracy. Thus, the following set of equations is defined based on applying n test frequencies $f_1, f_2, \ldots, f_n$ and observing the corresponding input impedances $|Z_{meas,f_1}|, |Z_{meas,f_2}|, \ldots, |Z_{meas,f_n}|$

$$\begin{cases} r_1 = \left|Z_{meas,f_1}\right| - \left|Z_T(f_1) + \frac{\left(2\pi f_1 k\sqrt{L_T L_R}\right)^2}{R+Z_R(f_1)}\right| = 0 \\ r_2 = \left|Z_{meas,f_2}\right| - \left|Z_T(f_2) + \frac{\left(2\pi f_2 k\sqrt{L_T L_R}\right)^2}{R+Z_R(f_2)}\right| = 0 \\ \vdots \\ r_n = \left|Z_{meas,f_n}\right| - \left|Z_T(f_n) + \frac{\left(2\pi f_n k\sqrt{L_T L_R}\right)^2}{R+Z_R(f_n)}\right| = 0. \end{cases} \tag{18}$$

It is noteworthy that $|Z_{in}|$ corresponding to each test frequency is calculated by dividing the rms of the inverter fundamental output voltage and the rms of i_T fundamental. By solving (18), the $|Z_{in}|$ curve given in (8) is fitted to the measured test points assuming that k, R_L, and C_R are unknown parameters. Therefore, solving (18) will end up estimating the parameters. To solve (18), the least-squares method is employed to provide an objective function. The Newton–Raphson method is used to minimize the objective function.

In this article, the first estimation is done using three test frequencies. Then, the fourth test frequency is applied and the second estimation is obtained consequently. If the results obtained from the first and second estimations are not close enough, it is concluded that the estimation accuracy is not sufficient. Therefore, another test frequency is applied and the estimation is run again until the estimated parameters converge to a specific value. From the above discussion, it is concluded that at least four test frequencies are applied during the proposed identification method. According to the fact that the distribution of these test frequencies contributes to the better accuracy of the estimation, the test frequencies are scattered evenly in Region II. The first four are determined as $f_1 = 70$ kHz, $f_2 = 78$ kHz, $f_3 = 86$ kHz, and $f_4 = 94$ kHz. If more test frequencies are needed to be applied to the system, the system follows $f_5 = 74$ kHz, $f_6 = 82$ kHz, $f_7 = 90$ kHz, and $f_8 = 98$ kHz. If the required accuracy is not achieved after applying eight frequencies, the series starts again by applying $f_1, f_2, \ldots, f_8$.

B. Control System

At the beginning of the system performance, the parameter estimation is performed, as described in Section V-A. For

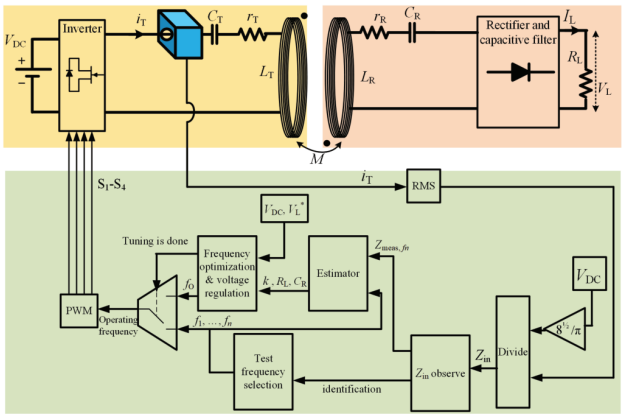

Fig. 5. Control block diagram of the control system proposed for parameter estimation and frequency optimization.

the sake of the frequency control, G values are calculated for a range of possible operating frequencies using (14) at first. The frequencies realizing the required load voltage are recorded for the next process. Then, ϕ is calculated for each recorded frequency using (17). Among them, the frequencies corresponding to $0° < \phi < 30°$ are recorded. η_{ac} is calculated for the recorded frequencies by using (10). The frequency resulting in highest η_{ac} is selected as the optimum frequency f_O and applied to the system. In this way, the WPT system provides the required load voltage while operating in soft switching and high efficiency. It is noteworthy that the method can be employed for tuned and detuned systems. The effect of detuning is considered in the control system as C_R is included in the estimated parameters of the system.

The control block diagram is given in Fig. 5. A multiplexer is controlled by the frequency optimization and voltage regulation unit. During the identification period, the multiplexer is switched in a way that the predefined test frequencies are passed to the PWM unit. The obtained $|Z_{in}|$ corresponding to each test frequency is given to the estimator. The estimated parameters are given to the frequency optimization and load voltage regulation unit. The frequency realizing ZVS, low conduction loss, and V_L^* is selected as the optimum frequency. Then, the multiplexer is switched in a way that passes the optimum frequency to the PWM unit.

It is noteworthy that k and R_L may change during operation, causing the determined f_O to deviate from the optimal value. Therefore, the identification and frequency optimization process needs to be rerun. For this purpose, $|Z_{in}|$ is observed during the system operation continuously. It is done by inspecting the change of $|Z_{in}|$ in a small time window and a large time window to observe abrupt and gradual changes, respectively. If the variation is larger than a threshold, it is interpreted as a result of a possible change in the system parameters. Then, the identification process starts again.

The new f_O is calculated based on the newly estimated parameters and applied to the system.

C. Gain Selection

Soft switching is achieved with proper designing of the system control incorporating load voltage regulation. In this

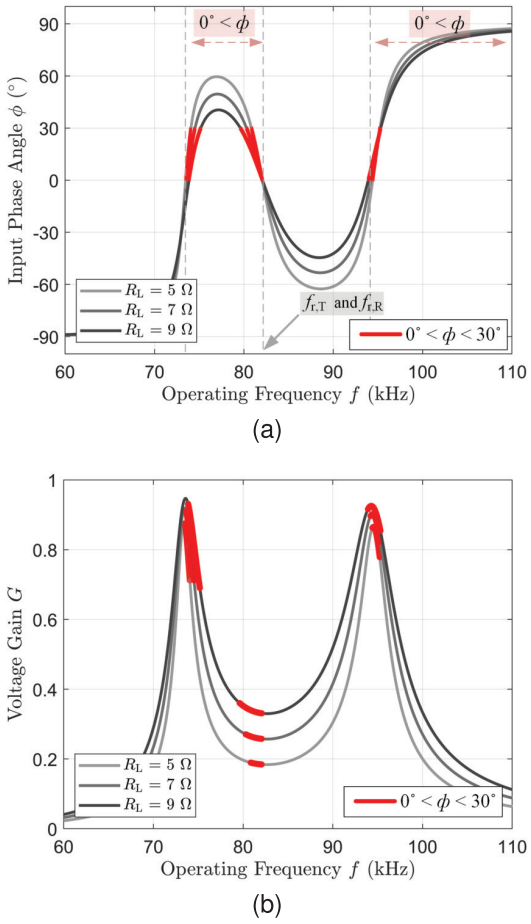

Fig. 6. Obtaining the desired operation points for optimum performance. (a) Input phase angle. (b) Voltage gain.

section, the considerations of selecting a suitable voltage gain G^*, resulting in V_L^* across the load are analyzed. Then, the input dc voltage of the system can be designed, so that the nominal load voltage of the system can be provided. As mentioned in Section IV, operation at the regions B and D results in ZVS. On the other hand, it is better to operate at the boundaries of Regions B and D to have a smaller input phase angle.

The selection is demonstrated in Fig. 6(a) by red markers. The frequency bands corresponding to $\phi > 0°$ realize ZVS [15]. The points corresponding to $\phi < 0°$ are ignored as they do not realize ZVS. Moreover, a limit of $\phi < 30°$ is set in order to avoid large input phase values, which cause higher power loss in the system. The selected operating points are reflected on the G curves in Fig. 6(b). As was expected, the selected operating points correspond to the maximum and minimum points of the voltage gain curves. The points around maximum G, which are common for all k values, are desirable for the nominal G. Meanwhile, variations of other parameters should be considered for the design of nominal G as well. Therefore, parameters k, R_L, and detuning corresponding to the case studies of this article are considered in Fig. 7(a). The operating points corresponding to $0° < \phi < 30°$ are depicted in Fig. 7(a) for $0.25 < k < 0.35$, $6.4\ \Omega < R_L < 21\ \Omega$ for both tuned and 5 % detuned cases. In this article, it is desired to achieve 40 V

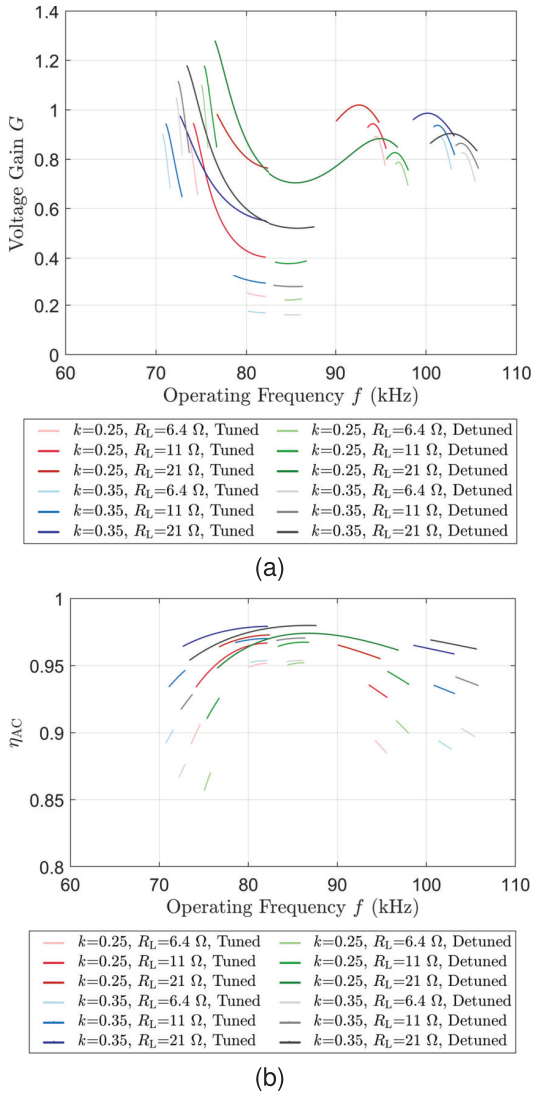

Fig. 7. Operating points corresponding to positive and low input phase angle for different values of k, R, and detuned resonant frequencies. (a) Voltage gain and (b) ac–ac efficiency of the system.

at the system load voltage. According to Fig. 7(a), $G = 0.8$ can be reached for different k, R_{L} values, as well as tuned and detuned cases. Therefore, V_{dc} can be set on 50 V to achieve $V_{\mathrm{L}} = 40$ V while $G = 0.8$.

In Fig. 7(b), the curves of η_{ac} are plotted for the operating points mentioned in Fig. 7(a). It is seen that for all of them, η_{ac} is higher than 85%. It is noteworthy that the proposed variable frequency method does not apply the frequency corresponding to maximum η_{ac} to the system. Meanwhile, the fact that the upper limit of input phase angle is set to 30° keeps the power loss attributed to the resonant circuit low. Therefore, η_{ac} is still high at the obtained operating points.

The operation range is analyzed in Fig. 8. for both tuned and deuned systems considering $0 < \phi < 30°$ and, $G = 0.8$, as defined in this study. In this paper, a 5% detuning, corresponding to $C_R = 20$ nF is defined as the maximum allowable detuning. Within this range, the load voltage regulation and low power loss remain feasible.

It is noteworthy that the bifurcation effect may happen due to different values of k and R_{L}. The effect can be seen in Figs. 3(a) and 6(a) as there are three frequencies resulting

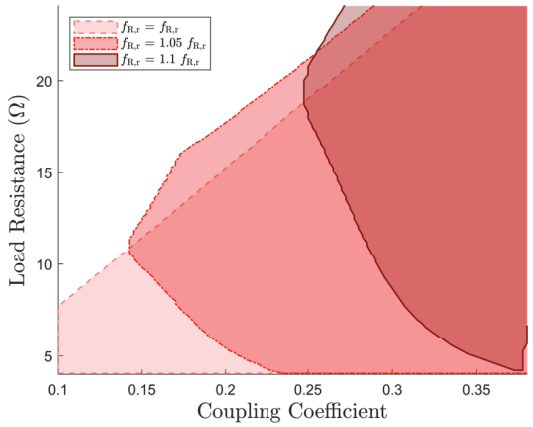

Fig. 8. System operation range realizing $G = 0.8$ and $0° < \phi < 30°$ for tuned and detuned cases.

in $\phi = 0°$ [22]. The proposed control system is able to find the optimum operating frequency regardless of the bifurcation. This is because the whole bandwidth is considered in the first step of the calculation, where G is calculated for each frequency. However, considering ZVS and low conduction power loss, only one frequency is selected as the optimum operating frequency.

D. Discussion

Overall, the advantages of the proposed method are given as follows.

1) No extra converters or components are added to the conventional WPT systems. Thus, the corresponding power loss and capital cost are avoided.
2) The proposed control system does not require data communication between the transmitter and receiver sides as it only uses the measurements of i_{T} and takes the control actions at the same side. This will increase the reliability of the system and decrease the capital cost.
3) The proposed method merely needs one sensor. It reduces the cost and complexity of the system.
4) Only the magnitude of the transmitter current is required for the operation. Therefore, the difficulties of the phase measurements are avoided.
5) The control method can deal with detuned cases as well as the variable k and R_{L} during operation. Thus, it can be employed for a wide range of applications.

VI. Validation

The proposed system identification and control method are validated experimentally in this section. An experimental WPT setup is implemented in the laboratory to evaluate the effectiveness of the proposed method. As shown in Fig. 9, it includes an H-bridge transmitter-side inverter, transmitter and receiver windings without ferrite bars and aluminum plates, a full bridge rectifier, a National Instruments Data Acquisition (NI-DAQ) board, and an ARM STM32F407 microcontroller for implementing the control method. A closed-loop Hall effect current transducer LTS-15NP is used as the current sensor. The sampling rate is 2 MHz. The circuit parameters of the system are designed based on the approach given in [21] and presented in Table II. In order to evaluate the effectiveness

TABLE III
ESTIMATION AND FREQUENCY OPTIMIZATION RESULTS

	Case 1	Case 2	Case 3	Case 4	Case 5	Case 6	Case 7
k	0.25	0.35	0.35	0.35	0.25	0.35	0.35
C_{R} (nF)	22	22	22	22	20	20	22
R_{L} (Ω)	11	11	21	6.4	11	11	65
Estimated k	0.25	0.34	0.36	0.39	0.25	0.34	0.38
Estimated C_{R} (nF)	21.79	21.63	21.89	21.69	19.80	19.73	22.18
Estimated R_{L} (Ω)	9.79	10.25	19.55	6.48	10.10	10.82	67
f_{O} (Hz) (analysis)	75150	72000	74570	71174	97450	105400	109680
f_{O} (Hz) (experimental)	74900	72900	74000	71680	98960	106200	110000
V_{L}^{*} (V)	40	40	40	40	40	40	40
Obtained V_{L} (V)	41	39	39.5	38	39	38	41
η_{exp} (%)	92	94	80	91	90	92	92

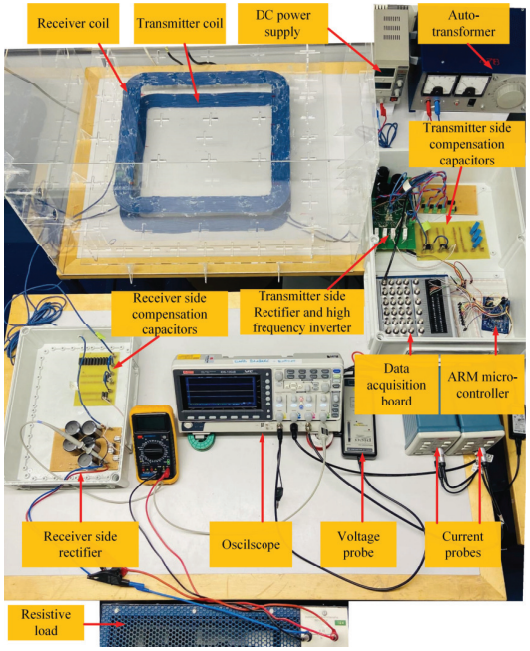

Fig. 9. Experimental setup of the WPT system implemented in laboratory.

of the method in different conditions, seven case studies are defined in this section and in Table III. In all of the cases, $V_{\mathrm{dc}} = 50$ V and $V_{\mathrm{L}}^{*} = 40$ V.

A. Tuned System With Constant R_L

For cases 1 and 2, the proposed estimation method is applied to the experimental system while $f_{\mathrm{T,r}} = f_{\mathrm{R,r}} = 82$ kHz and $R_{\mathrm{L}} = 11\ \Omega$. In case 1, the coupling coefficient is 0.25. The estimation results are shown in Table III. It is seen that the estimated values comply with the actual values with good accuracy. On the other hand, voltage regulation is carried out by the controller as well. It is seen that V_{L} stays at 41 V, which is close to $V_{\mathrm{L}}^{*} = 40$ V. The obtained frequency is 74 900 Hz, while the frequency corresponding to $G = 0.8$ is 75 150 Hz in the analytical result in Fig. 7(a). The resultant operating point is depicted in Fig. 10(a). It is seen that the positive phase angle of i_{T} with respect to the inverter voltage is realized. As shown in Fig. 10(a), MOSFETs Q_1 and Q_3 are turned on at the rising edge of the inverter output voltage waveform. Since the current is negative at that moment, it flows through D_1 and D_3. Therefore, the voltages across the drain and source of Q_1 and Q_3 are zero. The same phenomenon occurs for the

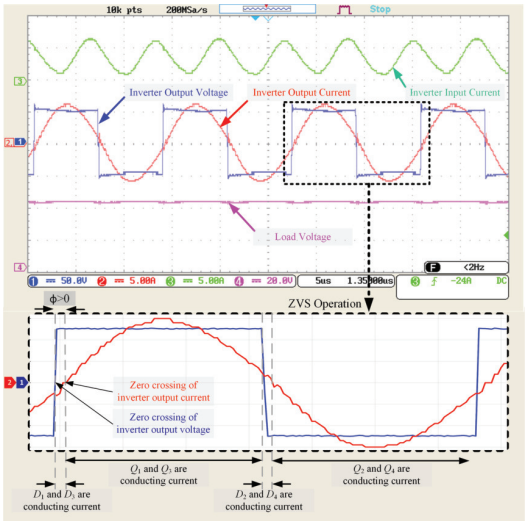

Fig. 10. Experimental results for the tuned WPT system while $R_{\mathrm{L}} = 11\ \Omega$: (a) case 1: $k = 0.25$ and (b) case 2: $k = 0.35$.

other IGBTs at the falling edge of the inverter output voltage waveform. Q_2 and Q_4 are turned on at the falling edge of the inverter output voltage waveform. Since the current is positive at that moment, it flows through D_2 and D_4. Therefore, the voltages across the drain and source of Q_2 and Q_4 are zero and the system operates at ZVS. On the other hand, the phase angle value is small, contributing to the low conduction loss in the whole system.

The coupling coefficient is changed to 0.35 in case 2. The required parameters are estimated as $k = 0.34$, $R_{\mathrm{L}} = 10.25\ \Omega$, and $C_{\mathrm{R}} = 21.63$ nF. Comparing the estimated and actual values in Table III, it is seen that the estimation has been successful. The controller also regulates the load voltage and stabilizes it

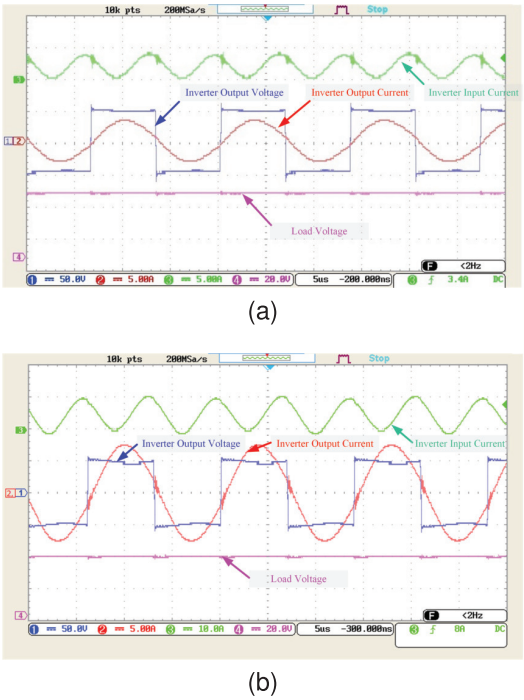

Fig. 11. Experimental results for tuned system while $k = 0.35$. (a) Case 3: $R_L = 21\ \Omega$ and (b) Case 4: $R_L = 6.4\ \Omega$.

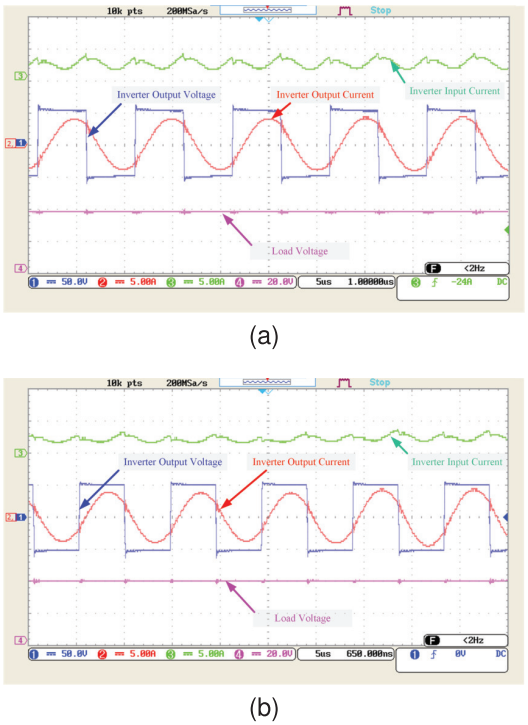

Fig. 12. Experimental results for the detuned WPT system while $f_{R,r} = 1.05\ f_{T,r}$ and $R_L = 11\ \Omega$. (a) Case 5: $k = 0.25$ and (b) Case 6: $k = 0.35$.

at 39 V. The obtained operating frequency is 72 900 Hz, while 72 000 Hz is the frequency that realizes $G = 0.8$ in theory. The corresponding waveforms are shown in Fig. 10(b). Similar to case 1, it is seen that the inverter current is lagging and the ZVS operation is still realized, consequently. Moreover, the conduction power loss is low due to the small phase difference.

B. Tuned System With Constant k

For the sake of validating system effectiveness under different R_L values, Cases 3 and 4 are defined, wherein $f_{T,r} = f_{R,r} = 82$ kHz and $k = 0.35$. In Case 3, $R_L = 21\ \Omega$. As seen in Table III, the estimator has calculated k, C_R, and R_L values accurately. Then, the optimum frequency is obtained as $f_O = 74$ kHz and applied to the system. As shown in Fig. 11(a), it is seen that 39.5 V is provided to the load. Furthermore, the resultant ϕ is positive and small that corresponds to ZVS operation and low conduction loss, respectively.

In Case 4, $R_L = 6.4\ \Omega$ while k, $f_{T,r}$, and $f_{R,r}$ have the same value as in Case 3. The results can be seen in Table III and Fig. 11(b). It is seen that the estimated values are close to the actual values. Applying $f_O = 71.68$ kHz to the system results in $V_L = 38$ V. The input phase angle is lightly inductive, which leads to both low switching and low conduction power loss for the system.

C. Detuned System

In Cases 5 and 6, the detuned systems are studied. For this purpose, C_R is reduced 9% to realize 5% difference between $f_{T,r}$ and $f_{R,r}$. With $k = 0.25$, the estimated values for Case 5 are given in Table III. The controller also regulates V_L at 39 V, which is close to the 40-V command. The obtained frequency is 98 960 Hz, which is close to the analytical result of 97 450 Hz for $G = 0.8$ in Fig. 7(a). Fig. 12(a) demonstrates the resultant operating point, which achieves a lagging phase angle of i_T with respect to the inverter voltage, corresponding to ZVS. The small phase angle value contributes to low conduction loss in the whole system.

In Case 6, $k = 0.35$. The estimated values presented in Table III are close to the actual ones. The controller regulates the voltage by setting the operating frequency at 106 200 Hz. It keeps V_L at 37 V, which is close to $V_L^* = 40$ V. In Fig. 7(a), it is seen that the required frequency for achieving the load voltage and soft switching is 105 400 Hz. In practice, Fig. 12(b) shows the resultant operating point achieving a positive phase angle of i_T, corresponding to ZVS. The small phase angle value contributes to low conduction loss in the whole system.

Overall, it is noted that ϕ is larger in the detuned cases compared with the tuned one. It can be understood from Fig. 7(a) as the frequency range realizing $0° < \phi < 30°$ is narrower for detuned cases. Moreover, the frequencies realizing $G = 0.8$ are located close to the right-side peak of the curve for detuned cases. Yet for tuned cases, the frequencies around both left- and right-side peaks can be selected for $G = 0.8$.

It is also desired to analyze the system efficiency, η_{exp} by averaging the product of the input voltage and current as the input power and V_L^2/R_L as the output power. The results are given in Table III for the six case studies. Except for the third case, the efficiency of the system is higher than 90%. In fact, the proposed control method of this article deviates the operating frequency from the one that realizes maximum efficiency in order to regulate the load voltage. Meanwhile, it is proven that the resultant efficiency is still high enough to be acceptable due to the fact that ZVS and low ϕ goals are considered alongside the load voltage regulation.

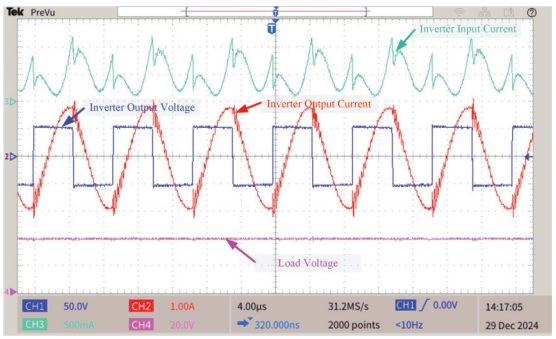

Fig. 13. Experimental results for Case 7, wherein $R_L = 65\ \Omega$, $k = 0.35$.

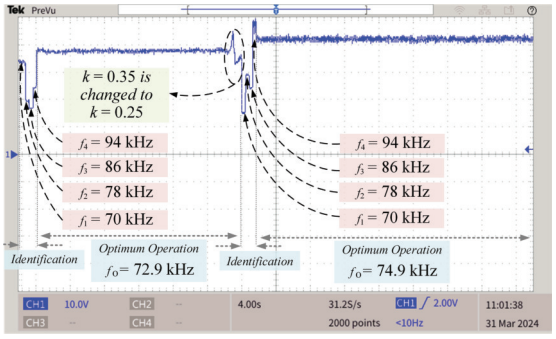

(a)

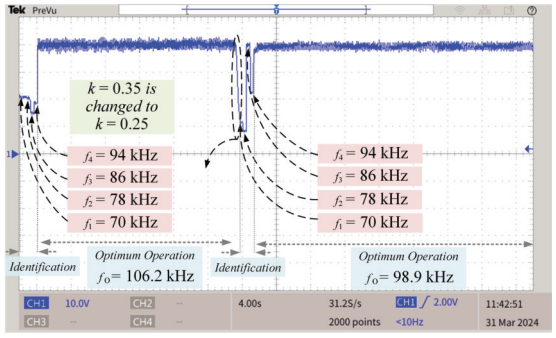

(b)

Fig. 14. Dynamic variation of system load voltage under the performance of the proposed control method with changing coupling coefficient while $R_L = 11\ \Omega$. (a) Tuned system and (b) detuned system $f_{R,r} = 1.05\ f_{T,r}$.

D. High R_L

The control system operation is validated experimentally in Case 7, wherein $R_L = 65\ \Omega$. The estimation results are given in Table III. It is seen that the system is able to estimate the parameters well. The optimum operating frequency is obtained as 110 kHz. The system waveforms are given in Fig. 13. As discussed in Section V-B, the upper limit of ϕ is ignored in this condition. It is seen that V_L is set on 41 V. The positive ϕ required for ZVS is realized. The system efficiency is calculated as 92%. This complies with the discussion in Section V-B, where it is claimed that η_{ac} is less sensitive to frequency variation for high R_L cases. It is seen that the controller is able to regulate V_L and realize ZVS operation, while the resultant efficiency is kept high.

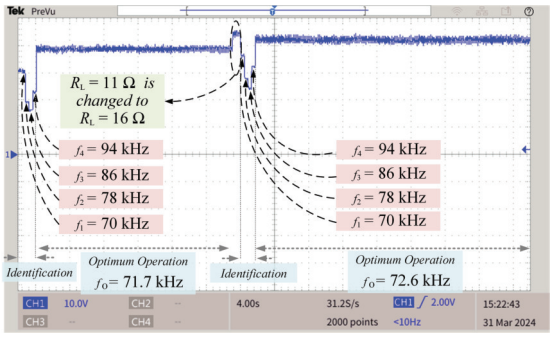

(a)

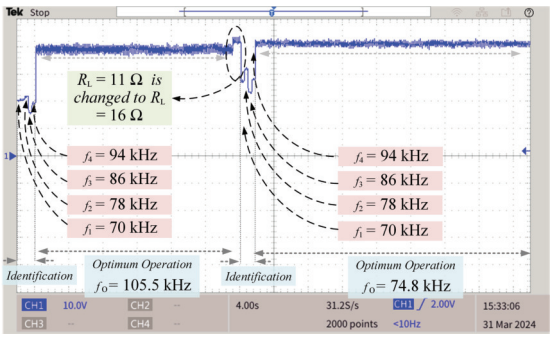

(b)

Fig. 15. Dynamic variation of system load voltage under the performance of the proposed control method with changing load resistance while $k = 0.35$. (a) Tuned system and (b) detuned system $f_{R,r} = 1.05\ f_{T,r}$.

E. Dynamic Performance Under Changing Coupling Coefficient

The dynamic performance of the system using the proposed control method is assessed using the experimental setup. As shown in Fig. 14(a), the system starts operation while $k = 0.35$ and $R_L = 11\ \Omega$. First, the control system applies three test frequencies, $f_1 = 70$ kHz, $f_2 = 78$ kHz, and $f_3 = 86$ kHz to estimate the parameters, as mentioned in Section V. Then, the fourth test frequency, $f_4 = 94$ kHz is applied to the system, and the estimation routine runs again. The selection process for the test frequency is explained in Section V. As the newly estimated results are close to the previous ones, the optimum frequency f_O realizing the 40-V load voltage, ZVS condition, and lowest ϕ is calculated according to the estimated parameters. As seen in 14(a), the load voltage reaches 38 V by applying $f_O = 72.9$ kHz.

As mentioned in Section V, $|Z_{in}|$ is continuously observed during the steady-state operation to detect the possible change of parameters. The system's capability to deal with the change of k is assessed by making a sudden intentional misalignment causing $k = 0.35$ to drop to $k = 0.25$. The resultant change in $|Z_{in}|$ is observed and interpreted as a change in system parameters. Thus, the identification method runs again. An estimation of new parameters is obtained after applying test frequencies. Then, $f_O = 74.9$ kHz is calculated as the new optimum frequency providing 41 V at the load while $V_L^* = 40$ V. The detuned system performance is shown in

Fig. 14(b) with the same test scenario. It is seen that V_L = 42 V by applying the updated optimum frequency, f_O = 98.9 kHz.

F. Dynamic Performance Under Changing the Load Resistance

Fig. 15(a) shows the dynamic performance while R_L changes from 11 Ω to 16 Ω. It is seen that the updated optimum frequency, f_O = 72.6 kHz realizes 41 V at the load. The detuned system performance is shown in Fig. 15(b) with the same test scenario. It is seen that V_L^* = 41 V by applying the updated optimum frequency, f_O = 73.2 kHz.

Overall, the obtained dynamic operations of the system at the six mentioned scenarios show that the control system is fast enough to find the optimum frequency even under variable k or R_L. Moreover, the system is also able to deal with detuned receivers as the estimator also calculates the C_R value. As seen in Figs. 14(a) and 15(a), the identification process takes almost 2 s at maximum. The detection of the parameter change is less than 1 s. Compared to the whole charging period which takes tens of minutes, the proposed method takes negligible time for identification. The accuracy of the identification process gets affected in practice if the test intervals of each test frequency are shortened. Meanwhile, using current sensors with higher bandwidth results in higher accuracy in shorter identification time. Moreover, employing powerful processors contributes to fast accurate estimation too. On the other hand, V_L^* is realized with good accuracy in the steady-state operation of the system. In the worst case, a 5% error of the voltage is observed for the system.

VII. Conclusion

An identification method for the estimation of coupling coefficient, equivalent load resistance, and detuning of transmitter and receiver resonant frequencies of WPT systems is proposed in this article. It is based on applying different test frequencies, measuring absolute value of the input impedance, and estimating the parameters using a nonlinear fitting method. Optimum frequency control is also proposed to regulate the load voltage, realize ZVS, and lower system conduction power loss. The whole identification and control process only needs a single current sensor at the transmitter side. Furthermore, the problem of phase measurement is avoided as only the magnitude of the current is needed. The system does not require data communication between the system's two sides and is able to deal with detuned cases and variable coupling coefficients during operation. The experimental results show that the provided load voltage is close to the reference value while the soft switching condition is met.

For future studies, the estimation method can be enhanced in a way that it estimates self-inductance of the receiver circuit as well as the rest of the parameters. Alternatively, a low-speed data communication link can be employed to transfer the accurate parameters of the receiver circuit to the controller located at the transmitter side. However, the reliability and cost of such a communication system remain concerns.

References

[1] A. Zakerian, S. Vaez-Zadeh, and A. Babaki, "A dynamic WPT system with high efficiency and high power factor for electric vehicles," *IEEE Trans. Power Electron.*, vol. 35, no. 7, pp. 6732–6740, Jul. 2020.

[2] R. K. Yakala, S. Pramanick, D. P. Nayak, and M. Kumar, "Optimization of circular coil design for wireless power transfer system in electric vehicle battery charging applications," *Trans. Indian Nat. Acad. Eng.*, vol. 6, no. 3, pp. 765–774, Sep. 2021.

[3] J. Yang, X. Zhang, K. Zhang, X. Cui, C. Jiao, and X. Yang, "Design of LCC-S compensation topology and optimization of misalignment tolerance for inductive power transfer," *IEEE Access*, vol. 8, pp. 191309–191318, 2020.

[4] Z. Luo, Y. Zhao, M. Xiong, X. Wei, and H. Dai, "A self-tuning LCC/LCC system based on switch-controlled capacitors for constant-power wireless electric vehicle charging," *IEEE Trans. Ind. Electron.*, vol. 70, no. 1, pp. 709–720, Jan. 2023.

[5] A. Babaki, S. Vaez-Zadeh, A. Zakerian, and G. A. Covic, "Variable-frequency retuned WPT system for power transfer and efficiency improvement in dynamic EV charging with fixed voltage characteristic," *IEEE Trans. Energy Convers.*, vol. 36, no. 3, pp. 2141–2151, Sep. 2021.

[6] K. Chen, K. W. E. Cheng, Y. Yang, and J. Pan, "A fast self-positioning-based optimal frequency control for inductive wireless power transfer systems without communication," *IEEE Trans. Ind. Electron.*, vol. 70, no. 1, pp. 334–343, Jan. 2023.

[7] K. Wang, J. Zeng, Y. Yang, and S. Y. R. Hui, "A general maximum energy efficiency tracking scheme for domino wireless power transfer systems with quasi-load-independent outputs," *IEEE Trans. Power Electron.*, vol. 39, no. 1, pp. 1840–1852, Jan. 2024.

[8] L. Wang et al., "Mutual inductance identification of IPT system based on soft-start process," *IEEE Trans. Power Electron.*, vol. 37, no. 6, pp. 7504–7517, Jun. 2022.

[9] K. Chen, Z. Nie, C. Yan, N. C. Cheung, E. K.-W. Cheng, and J. Pan, "A noncommunication mutual inductance estimation method for multiple transmitters SS-compensated dynamic wireless power transfer with low calculation effort," *IEEE Trans. Power Electron.*, vol. 39, no. 7, pp. 7803–7807, Jul. 2024.

[10] K. Li, H. Yuan, S.-C. Tan, and S. Y. R. Hui, "Overshoot damping and dynamics improvement in wireless power transfer systems via receiver-side controller design," *IEEE Trans. Power Electron.*, vol. 37, no. 2, pp. 2362–2371, Feb. 2022.

[11] Y. Xiao and C. Liu, "Direct load voltage control for electrolytic capacitorless wireless power transfer system without DC/DC converter," *IEEE Trans. Ind. Electron.*, vol. 68, no. 9, pp. 8039–8048, Sep. 2021.

[12] M. Wu et al., "A dual-sided control strategy based on mode switching for efficiency optimization in wireless power transfer system," *IEEE Trans. Power Electron.*, vol. 36, no. 8, pp. 8835–8848, Aug. 2021.

[13] A. F. A. Aziz, M. F. Romlie, and T. Z. A. Zulkifli, "CLL/S detuned compensation network for electric vehicles wireless charging application," *Int. J. Power Electron. Drive Syst.*, vol. 10, no. 4, p. 2173, Dec. 2019.

[14] H. Feng, T. Cai, S. Duan, X. Zhang, H. Hu, and J. Niu, "A dual-side-detuned series–series compensated resonant converter for wide charging region in a wireless power transfer system," *IEEE Trans. Ind. Electron.*, vol. 65, no. 3, pp. 2177–2188, Mar. 2018.

[15] P. Zhao, J. Liang, H. Wang, and M. Fu, "Detuned LCC/S-S compensation for stable-output inductive power transfer system under UltraWide coupling variation," *IEEE Trans. Power Electron.*, vol. 38, no. 10, pp. 12342–12347, Oct. 2023.

[16] R. Matsumoto and H. Fujimoto, "Adaptive compensation scheme for wireless power transfer systems with coil inductance variation using PWM-controlled switched capacitor," in *Proc. Wireless Power Week (WPW)*, Bordeaux, France, Jul. 2022, pp. 244–248.

[17] F. Grazian, T. B. Soeiro, and P. Bauer, "Inductive power transfer based on variable compensation capacitance to achieve an EV charging profile with constant optimum load," *IEEE J. Emerg. Sel. Topics Power Electron.*, vol. 11, no. 1, pp. 1230–1244, Feb. 2023.

[18] S. N. Kalat, S. Vaez-Zadeh, A. Zakerian, A. Babaki, and T. Ebel, "A communication-free and model-free predictive control for a dynamic IPT system with high power factor for electric vehicles," *IEEE Access*, vol. 11, pp. 96773–96783, 2023.

[19] L. He and D. Guo, "An active switched-capacitor half-wave receiver with high efficiency and reduced components in WPT system," *IEEE Trans. Ind. Electron.*, vol. 68, no. 12, pp. 12119–12129, Dec. 2021.

[20] N. Fu, J. Deng, Z. Wang, and D. Chen, "Dual-phase-shift control strategy with switch-controlled capacitor for overall efficiency optimization in wireless power transfer system," *IEEE Trans. Veh. Technol.*, vol. 72, no. 6, pp. 7304–7317, Jun. 2023.

[21] Y. Jiang, L. Wang, Y. Wang, J. Liu, M. Wu, and G. Ning, "Analysis, design, and implementation of WPT system for EV's battery charging based on optimal operation frequency range," *IEEE Trans. Power Electron.*, vol. 34, no. 7, pp. 6890–6905, Jul. 2019.

[22] P. Sun et al., "Analysis of frequency bifurcation and frequency splitting of IPT system under overcoupling," in *Proc. 4th Int. Conf. Clean Energy Electr. Syst.*, vol. 8, May 2022, pp. 61–72.

Ali Zakerian received the B.Sc. degree in electrical engineering (power) from K. N. Toosi University of Technology, Tehran, Iran, in 2016, and the M.Sc. degree in power electronics and electrical machines from the University of Tehran, Tehran, in 2019. He is currently pursuing the Ph.D. degree in power electronics with Tampere University, Tampere, Finland.

He has been actively studying wireless power transfer systems since 2017. He also has professional experience in both the marine and power systems industries. He worked as an Application Engineer at WE Tech Solutions Oy, Vaasa, Finland, where he developed power and energy management systems for hybrid merchant vessels. He is currently a Control Engineer at General Electric, Tampere, Finland, focusing on control software for STATCOM and SVC systems. His research interests include wireless power transfer, system identification, power and energy management systems, flexible ac transmission systems (FACTS), and grid stability.

Sohrab Abbasian (Graduate Student Member, IEEE) was born in Babol, Iran, in 1995. He received the B.Sc. degree from Babol Noshirvani University of Technology, Babol, in 2018, and the M.Sc. degree in electrical power engineering (power electronics) from the K. N. Toosi University of Technology, Tehran, Iran, in 2021. He is currently pursuing the Ph.D. degree in power electronics engineering with Tampere University, Tampere, Finland.

Since May 2024, he has been working as a Research and Development Engineer at Eaton Electric, Vantaa, Finland. His research interests include ac–dc and dc–dc power converters, high-gain dc–dc converters, soft-switching techniques for dc–dc converters, and renewable energy conversion.

Prasad Jayathurathnage (Senior Member, IEEE) received the B.Sc. degree in electronics and telecommunications engineering from the University of Moratuwa, Moratuwa, Sri Lanka, in 2009, and the Ph.D. degree in electrical and electronic engineering from Nanyang Technological University, Singapore, in 2017.

From 2017 to 2018, he was a Research Fellow with the Queensland University of Technology, Brisbane City, QLD, Australia, and Rolls-Royce-NTU Corporate Lab, Singapore. From 2018 to 2023, he was a Full-Time Post-Doctoral Researcher with the School of Electrical Engineering, Aalto University, Espoo, Finland, and an Academic Guest with the Power Electronic Systems Laboratory, ETH Zürich, Zürich, Switzerland. He is currently a Senior Research Engineer with Danfoss Drives, Tampere, Finland. He has authored more than 60 research articles in various journals, conferences, and tutorial seminars. His research interests include high-frequency power converters, wide-bandgap devices, passive components, and wireless power transfer.

Dr. Jayathurathnage was a recipient of several accolades for his research, including the Best Paper Awards at IEEE PEMC 2018, IEEE ISMICT 2019, and IEEE SPEC 2022.

Tomi Roinila (Member, IEEE) received the M.Sc. (Tech.) and Dr. (Tech.) degrees in automation and control engineering from Tampere University of Technology, Tampere, Finland, in 2006 and 2010, respectively.

He is currently an Associate Professor at Tampere University, Tampere. His main research interests include the modeling and control of grid-connected power electronic systems, analysis of energy storage systems, and modeling of multiconverter systems.

Marcelo Godoy Simões (Fellow, IEEE) received the B.Sc. and M.Sc. degrees from the University of São Paulo, São Paulo, Brazil, and the Ph.D. degree from The University of Tennessee, Knoxville, TN, USA, in 1985, 1990, and 1995, respectively, and the D.Sc. degree (Livre-Docência) from the University of São Paulo, in 1998.

He has been a Professor of flexible and smart power systems at the University of Vaasa, Finland, since 2021. He is a Pioneer to apply neural networks and fuzzy logic in power electronics, motor drives, and renewable energy systems. His fuzzy logic-based modeling and control for wind turbine optimization is used as a basis for advanced wind turbine control and it has been cited worldwide. His leadership in modeling fuel cells is internationally and highly influential in providing a basis for further developments in fuel cell automation control in many engineering applications. He made substantial and lasting contribution of artificial intelligence technology in many applications, power electronics and motor drives, fuzzy control of wind generation system, such as fuzzy logic-based waveform estimation for power quality, neural network-based estimation for vector-controlled motor drives, and integration of alternative energy systems to the electric grid through AI modeling-based power electronics control. His current research interests intersect the areas of power electronics, power systems, power quality, smart grid, and renewable energy systems.

Dr. Simões was an U.S. Fulbright Fellow for AY 2014–2015, working for Institute of Energy Technology, Aalborg University, Aalborg, Denmark. He was elevated to the grade of IEEE Fellow, with the citation: "for Applications of Artificial Intelligence in Control of Power Electronics Systems."

Paavo Rasilo (Member, IEEE) received the M.Sc. (Tech.) and D.Sc. (Tech.) degrees from Helsinki University of Technology (currently Aalto University), Espoo, Finland, in 2008 and 2012, respectively.

He is currently working as a Professor of electromechanics at the Electrical Engineering Unit, Tampere University, Tampere, Finland. His research interests include computational electromagnetics and magnetic material modeling related to electrical machines, passive magnetic components, wireless power transfer, and energy harvesting.